



CrossMark
click for updates

Cite this: *RSC Adv.*, 2015, 5, 4615

Novel asymmetrical single- and double-chiral liquid crystal diads with wide blue phase ranges†

Chong-Lun Wei,^a Te-Cheng Chen,^a Putikam Raghunath,^b Ming-Chang Lin^b and Hong-Cheu Lin^{*a}

In this study, two series of novel asymmetrical single- and double-chiral liquid crystal diads using a central linker to link two different mesogenic cores were successfully synthesized. The effects of the position of chiral centers and the number of aromatic rings on the mesomorphic and electro-optical properties were investigated. We found that diads III-N (where N = A, B, C and D) have better mesophasic properties than II-N (where N = A, B, C, D and E). Compared with III-C with a chiral center at the terminal alkoxy chain, diad III-D exhibited the widest temperature range of BPI (*ca.* 31 °C) as the chiral center was introduced to the central linker. Besides III-D, BPs were also observed in diads II-B and III-B with a chiral center at the central spacer. According to our experimental results and molecular modeling, the mesomorphic properties and temperature ranges of BPs will be affected by the values of biaxiality and dipole moment, along with the bent shape of molecular geometry. Therefore, we demonstrated the first example of asymmetrical single- and double-chiral liquid crystal diads involved chiral centers located at the central linker to exhibit BPs, including the mesophases of BPI and BPIII, which might offer new BP single-components to the future applications of eutectic liquid crystal mixtures with wide BP ranges.

Received 6th November 2014
Accepted 5th December 2014

DOI: 10.1039/c4ra13943g

www.rsc.org/advances

Introduction

It is well known that liquid crystal molecules may reveal many different mesophases, including nematic,¹ smectic,² cholesteric,³ and blue phases, and these are attributed to their chemical structures, such as molecular configurations with specific shapes and dipole moments. Among these mesophases, blue phase liquid crystals (BPLCs) are observed between isotropic phase and chiral nematic (N*) phase during cooling process, which have less applications due to their narrow mesophasic ranges (usually about 1 K).⁴ It has been reported that BPLCs aggregate into internal helical alignments called “double twist cylinders (DTC)”,^{5,6} where are three types of BPLCs: blue phase I (BPI), blue phase II (BPII) and blue phase III (BPIII). The packing structures of these three BPLCs are described as follows: BP I is a body-center cubic structure, BP II is a simple cubic structure,^{7,8} and BP III is the same symmetry as the isotropic phase with arbitrary orientation.^{9,10} BPLCs have different performances in the field of optoelectronics: among all BPs, BP III has the fastest response speed,¹¹ and BP II shows smaller hysteresis and faster response time than BP I.¹² Though

very narrow ranges of BPLCs were observed, polymer stabilized BPLCs was first discovered by Kikuchi *et al.* to extend the temperature range of BPs phase over 60 °C.¹³ Since BPLC arrangements were stabilized by the polymer network design to enlarge the BPLC ranges, general interests have been attracted to develop BPLCs recently. Some advantages in the fields of optoelectronics and photonics are listed as follows:^{14,15} fast response time (about sub-millisecond), no alignment layer required,¹⁶ and free of typical birefringence.¹⁷

Nowadays, several research groups have reported numerous methods to induce the blue phase and enlarge the temperature range of blue phase, which were accomplished either by structural modifications or mixture optimizations. For example, Yang *et al.* utilized hydrogen bonds to stabilize BPLCs, where two complimentary hydrogen-bonded moieties were self-assembled by hydrogen bonds to form a BP complex with a wide temperature range about 23 °C.¹⁸ In addition, they also tried to dope hydrogen-bonded bent-shaped and T-shaped molecules to stabilize BPs.¹⁹ Pivnenko *et al.* synthesized bimesogens structures to induce BPLCs with a BP temperature range *ca.* 44 °C.²⁰ Besides, U-shaped molecules have also been doped with a chiral additive to extend the BP range successfully.²¹ There are some reports demonstrated that several biaxial nematic LCs doped with certain amounts of chiral materials can enhance the temperature range of BPs.^{22–24} Although BPLCs have so many benefits, very limited single-component BPLC molecules with wide BPLC ranges have been developed so far.

^aDepartment of Materials Science and Engineering, National Chiao Tung University, Hsinchu, Taiwan, Republic of China. E-mail: linhc@mail.nctu.edu.tw

^bCenter for Interdisciplinary Molecular Science, Department of Applied Chemistry, National Chiao Tung University, Hsinchu, Taiwan, Republic of China

† Electronic supplementary information (ESI) available. See DOI: 10.1039/c4ra13943g

Lately, many experts have designed special molecular structures with different shapes to exhibit or stabilize BPLC mesophases: rod-like,²⁵ bent-core,²⁶ T-shape,²⁷ discotic²⁸ and (asymmetrical or symmetrical) diad²⁹ architectures. Yoshizawa *et al.* used a binaphthyl structure to stabilize the blue phase with a temperature range of 30 °C approximately,³⁰ interestingly, various structures of liquid crystal diads have been reported,^{31–34} but the mesophasic behavior of liquid crystals almost only showed the nematic or smectic phases. However, Takezoe *et al.* linked a flexible spacer between a rod and a cholesterol mesogenic unit which exhibited a wide range of BPs.³⁵ Our previous research also reported a bent-core oxadiazole-based liquid crystal to possess a blue phase with a wide range of *ca.* 30 °C.³⁶

In this study, we synthesized two series of novel asymmetrical single- and double-chiral liquid crystal diads with an odd-number spacer to link two different mesogenic rods and introduced chiral centers into the central linker and/or flexible terminus of the diads. We demonstrated the effects of the number of aromatic rings and the positions of the chiral centers on the mesophasic behaviors of LCs. Interestingly, we found one of the double-chiral liquid crystal diad exhibited BPI with a wide temperature range about 31 °C. Moreover, the phase transition sequences, electric-optical properties, Kerr constants and theoretical calculations of molecular modeling were investigated in this report.

Experimental

Spectroscopic analysis

¹H NMR spectra were recorded on a Bruker Unity 300 MHz spectrometer using DMSO-d₆, CDCl₃ and THF-d₈ as solvents. Elemental analyses (EA) were performed on a Heraeus CHN-OS RAPID elemental analyzer. Synchrotron powder X-ray diffraction (XRD) measurements were performed at beam-line BL17A equipped with magnetic of the National Synchrotron Radiation Research Center (NSRRC), Taiwan, where the wavelength of X-ray was 1.33336 Å. The powder samples were packed in a capillary tube and heated by a heat gun, for which the temperature controller is programmable by a PC with a PID feedback system. The scattering angle theta was calibrated by a mixture of silver behenate and silicon.

Molecular simulation method

The gas phase optimization of all asymmetrical structures of liquid crystal diads **II-N** (N = A, B, C, D and E) and **III-N** (where N = A, B, C and D) was carried out with the generalized gradient approximation (GGA) density functional B97D along with dispersion correction³⁷ using the standard 6-31G(d,p) basis set. The predicted minima were further confirmed by frequency calculations at the same level. Only the lowest energy conformations are reported here. The electrostatic potential derived charges (ESP) were calculated according to Merz–Singh–Kollman (MK) scheme³⁸ at the B97D/6-31G(d,p) level of theory. ESP results were used to compute maps of electrostatic potential. The results of all the calculations reported in this work were

obtained using the Gaussian 09 *ab initio*/DFT quantum chemical package.³⁹

Liquid-crystalline and physical properties

The phase transition behaviors of all final asymmetrical diads were characterized by polarizing optical microscopy (POM) using a Leica DMLP equipped with a temperature control hot stage (Mettler Toledo FP82HT). Temperatures and enthalpies of phase transitions were determined by differential scanning calorimetry (DSC, model: Perkin Elmer Pyris 7) under N₂ at a heating and cooling rate of 1 °C min⁻¹. The performance of optical properties was determined in the range of blue phase temperature and the optical transmittance was studied with a function of applied electric AC field at 2 kHz. The transmittance with 100% and 0% were calibrated by that the cell under parallel polarizers. The distance between electrodes was 10 μm and the cell gap was maintained at 7.5 μm by spacers.

Preparation of materials

(i) (*S*)-6-((4'-Cyano-[1,1'-biphenyl]-4-yl)oxy)-4-methylhexyl 4-((4-((*R*)-octan-2-yloxy)benzoyl)oxy)benzoate, (**III-D**). The synthesis of compound **III-D** was shown in Scheme 1. To a stirred solution of **M1** (3.0 g, 9.7 mmol), **M2** (2.42 g, 4.9 mmol) and 4-(*N,N*-dimethylamino)pyridine (DMAP) (0.13 g, 1.06 mmol) in dry dichloromethane (100 mL), *N,N*-dicyclohexylcarbodiimide (DCC) (2.35 g, 11.6 mmol) was added and the reaction mixture stirred at room temperature overnight under nitrogen. The resulting precipitate of dicyclohexylurea (DCU) was filtered off and washed with an excess of dichloromethane (20 mL). The solvent was evaporated and the crude product was purified by silica gel chromatography (*n*-hexane/dichloromethane = 1 : 1 v/v) and then recrystallized from methanol/dichloromethane (5 : 1 v/v) to afford compound **III-D** as a white solid in 78% yield. ¹H NMR (300 MHz, CDCl₃): δ (ppm) 8.27 (d, *J* = 8.7 Hz, 2H), 8.17 (d, *J* = 8.7 Hz, 2H), 8.14 (d, *J* = 9.0 Hz, 2H), 7.71–7.63 (m, 4H), 7.54 (d, *J* = 8.7 Hz, 2H), 7.40 (d, *J* = 8.7 Hz, 2H), 7.31 (d, *J* = 9.0 Hz, 2H), 7.02–6.98 (m, 4H), 4.53–4.51 (m, 1H), 4.37 (t, *J* = 6.3 Hz, 2H), 4.09 (m, 2H), 1.92–1.84 (m, 5H), 1.52–1.33 (m, 15H), 1.35 (d, *J* = 6.6 Hz, 3H), 0.91 (t, *J* = 6.6 Hz, 3H). Anal. calcd for C₄₉H₅₁NO₈: C, 75.27, H, 6.57, N, 1.79; found: C, 75.31, H, 6.62, N, 1.83%.

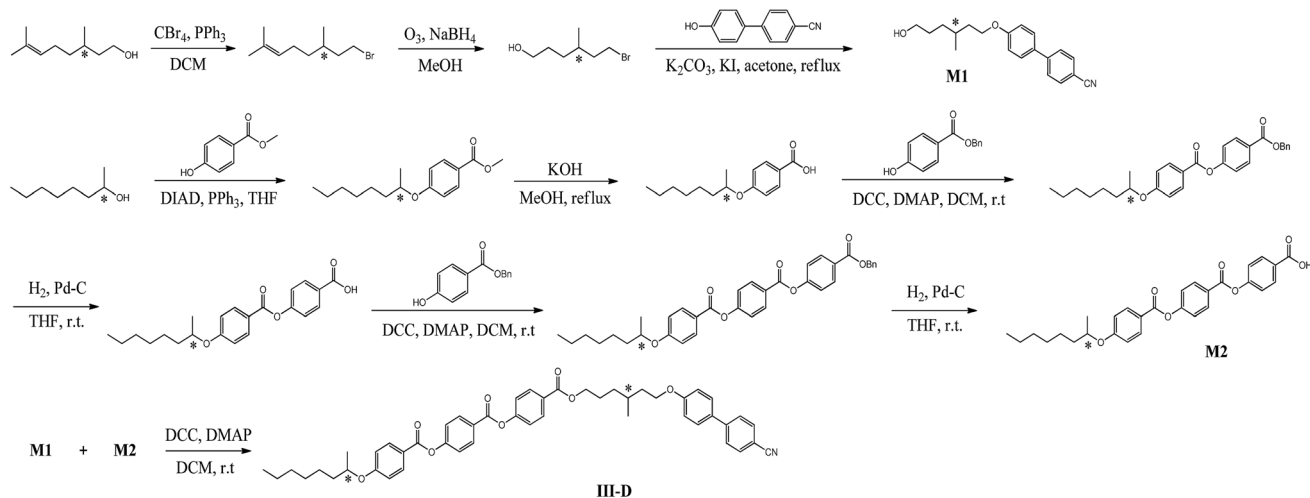
Results and discussion

Chemical synthesis

As illustrated in Fig. 1, series **II-N** (where N = A, B, C, D and E) and **III-N** (where N = A, B, C and D) were synthesized according to Schemes S1–S4 (see the ESI†), where one of the mesogenic rods in series **III** are longer than series **II**, along with B, C and D represent single- and double-chiral diads, respectively. These compounds with high purities were fully characterized by ¹H- and ¹³C-NMR, as well as mass ESI spectra (see the ESI†.)

Mesophasic and thermal properties

As shown in Table 1, the phase transition temperatures, enthalpies and mesophasic ranges of the asymmetrical liquid



Scheme 1 Synthesis of III-D.

crystal diads were determined by differential scanning calorimetry (DSC) and polarizer optical microscope (POM). The transition temperature of BPs–chiral nematic (N^*) was determined by POM (at a cooling rate of $0.5\text{ }^\circ\text{C min}^{-1}$) due to their undetectable enthalpy changes by DSC. To realize the effect of various asymmetrical configurations, including different numbers (or positions) of chiral centers and aromatic rings, on mesophasic and thermal properties of these asymmetrical single- and double-chiral liquid crystal diads, the comparison of all compounds are described as follows:

(i) **Compounds II-N (where N = A, B, C, D and E).** Compound II-A (no chiral center) exhibits a phase transition sequence of iso–nematic (N)–smectic A (SmA)–crystal. We tried to introduce a single chiral center to the central linker and flexible terminus of diads II-B and II-C, respectively. In contrast to II-C, diad II-B revealed BPIII (ranging $3.4\text{ }^\circ\text{C}$) due to the chiral center located at the central spacer, which induced twisting

power but didn't diminish the interactions of mesogenic cores. However, as the chiral center was shifted to the terminal alkoxy chain, the mesophases were totally vanished in II-C due to a stronger chiral twisting of the chiral center closer to the rigid core. Moreover, we also introduced double chiral centers to both central linker and flexible terminus of diad II-D, which do not have any mesophases due to even a stronger chiral twisting than II-C to further eliminate mesogenic interactions of mesophases. The strongest chiral twisting of both diads II-C and II-D to reduce the mesogenic interactions of rigid cores were also evidenced by their lowest crystallization (as well as isotropization) temperatures among all diads. Among these described chiral diads (II-B, II-C and II-D), only diad II-B with a single chiral center at the central spacer displayed mesophases, including BPIII. Hence, another single chiral diad II-E was introduced to investigate the effects of chiral center position at the central spacer, which showed a phase transition sequence of iso– N^* –crystal. Diad II-E with a chiral center at the central spacer possessed a mesophase of N^* , but BPIII was absent in II-E due to the different location of chiral center in contrast to II-B. Accordingly, a single chiral center located at the appropriate position of the central linker was required for diad II-B to obtain BPIII.

(ii) **Compounds III-N (where N = A, B, C and D).** The phase transition sequence of compound III-A is similar to II-A, *i.e.*, iso– N –SmA–crystal, but III-A has higher transition temperatures and wider mesophasic ranges (*i.e.*, N and SmA) than II-A due to the longer rigid core of III-A with a stronger π – π interaction. Similar to II-B and II-C, a single chiral center was introduced to the central spacer and flexible terminus of diads III-B and III-C, respectively. In comparison with III-C, single-chiral diad III-B exhibited BPI (ranging $1.5\text{ }^\circ\text{C}$) due to the chiral center located at the central spacer. Nevertheless, as the chiral center was shifted to the terminal alkoxy chain, III-C had similar mesophases of III-B, *i.e.*, N^* and SmA, but BPI was totally disappeared in III-C due to a stronger chiral twisting of the chiral center closer to the rigid core. Because of the same reason, compared with III-B,

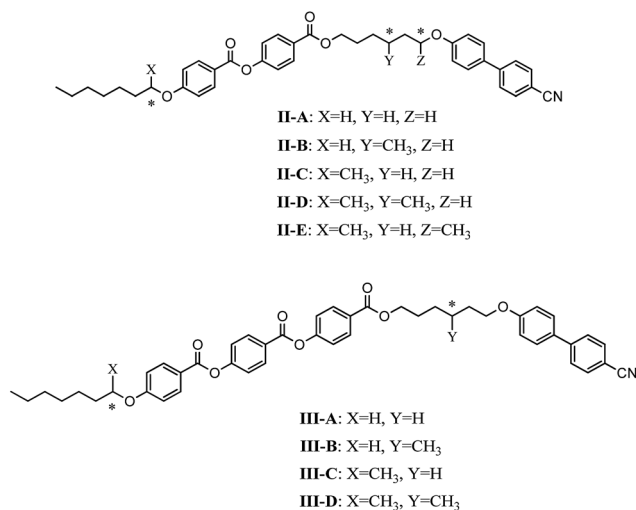


Fig. 1 Chemical structures of compounds II-N (where N = A, B, C, D and E) and III-N (where N = A, B, C and D).

Table 1 Phase transition temperatures (°C) and enthalpies (J g⁻¹) of asymmetrical liquid crystal diads^{a,b}

Compound	Phase transition temperature (°C) [enthalpies (J g ⁻¹)]	ΔT_{BP} (°C)	ΔT_{N^*} (°C)	ΔT_N (°C)	ΔT_{SmA} (°C)
II-A	Iso 99.2 [0.41] N 68.7 [1.89] SmA 36.6 [2.03] Cr			30.5	32.1
II-B	Iso 93.8 [0.54] BPIII 90.4 ^c N* 70.4 [2.31] SmA 44.3 [2.11] Cr	3.4	20.0		26.1
II-C	Iso 23.8 [3.57] Cr				
II-D	Iso 24.9 [16.11] Cr				
II-E	Iso 41.8 [0.10] N* 30.9 [0.83] Cr		10.9		
III-A	Iso 195.0 [1.12] N 119.1 [2.99] SmA 63.0 [1.51] Cr			75.9	56.1
III-B	Iso 182.2 [0.94] BPI 180.7 ^c N* 106.2 [2.44] SmA 72.5 [1.22] Cr	1.5	74.5		33.7
III-C	Iso 109.5 [11.76] N* 87.6 [5.43] SmA 79.7 [2.03] Cr		21.9		7.9
III-D	Iso 108.0 [0.36] BPI 76.6 ^c N* 51.9 [1.63] Cr	31.4	24.7		

^a Peak temperatures in the DSC profiles obtained during the first heating and cooling cycles at a rate of 1 °C min⁻¹. ^b Iso = isotropic phase; BPIII = blue phase III; BPI = blue phase I; N = nematic phase; N* = chiral nematic phase; SmA = smectic A phase; Cr = crystal. ^c The transition to this phase was observed under the polarizing optical microscope and it was too weak to be recognized by the DSC. (Phase transition temperatures and enthalpies of heating process are shown in Table S1.)

most transition temperatures and both mesophasic ranges of N* and SmA were reduced in **III-C**. Accordingly, SmA was totally removed and BPI (ranging 31 °C) was induced in double-chiral diad **III-D** owing to the introduction of double chiral centers to both central spacer and flexible terminus. Similarly, the strongest chiral twisting of diad **III-D** to decrease the mesogenic interactions of rigid cores was also evidenced by its lowest phase transition temperatures among all diads in series **III**.

(iii) Comparison of series II and III. All phase transition temperatures of the corresponding phases in compounds **III-N** were higher than those of compounds **II-N** (where N = A, B, C, D and E) because of the longer rigid core of series **III-N** (where N = A, B, C and D) with stronger π - π interactions. Among all diads, only diads **II-C** and **II-D** did not have any mesophases owing to their strongest chiral twisting with less mesogenic interactions of shorter rigid cores. In contrast to **II-C** and **II-D**, compounds **III-C** and **III-D** with a longer rigid core possessed stronger π - π interactions to compensate the chiral twisting thus to preserve the molecular assembly of mesophases. Interestingly, among all asymmetrical diads, BPs only existed in single-chiral diads **II-B**, **III-B** and double-chiral diad **III-D**, which all possessed chiral centers at central spacer. Compared with BPIII of **II-B**, the other diads **III-B** and **III-D** possessed BPI owing to their longer rigid core. Above all, double-chiral diad **III-D** was discovered to possess the widest BP temperature range among all diads, which is the first molecular design of liquid crystal diad with double-chiral centers (at both central spacer and flexible terminus) in the literature.

Optical and XRD investigations

Regarding the blue phases of diads **II-B**, **III-B** and **III-D**, we investigated the phase transitions by POM on cooling process (cooling rate 0.5 °C min⁻¹). Fig. 2(a)–(d) show the phase transitions of iso-BPIII-N*-SmA in **II-B**, respectively. In addition,

the POM texture of **III-B** at 181.0 °C upon cooling (0.5 °C min⁻¹) is also illustrated in Fig. S1.† Meanwhile, the phase transitions of iso-BPI-N* in **III-D** are shown in Fig. 3(a)–(c), respectively. All phase transitions were investigated by XRD measurements and their related data are shown in Fig. S2† and Table S2† of the ESI. Generally, sharp reflection peaks of XRD patterns (representing layer *d*-spacings) were observed in the small angle area of the smectic phase (including SmA), but only broad peaks were revealed in the wide angle area of the N and N* phases. As shown in Table S2† (see the ESI), **II-A** and **II-B** possessed *d*-spacing values of 41.8 Å and 43.4 Å, respectively. In addition, **III-A**, **III-B** and **III-C** also exhibited *d*-spacing values of 49.7 Å, 50.1 Å and 45.7 Å, respectively. Their *d*-spacing values (*d*) were a little larger than their corresponding molecular lengths (*L*) by the theoretical simulation (shown below), which suggested the *d*-spacing values of the SmA phase in these diads are interdigitated layer arrangements (*i.e.*, $L < d < 2L$). Therefore, the SmA phase was verified not only by the focal-conic fan texture of POM photographs but also by the *d*-spacing values of sharp reflection peaks.

The **II-B** behavior of BPIII could be verified by the rotation of the polarizer (see Fig. 4). As the polarizer was rotated clockwise

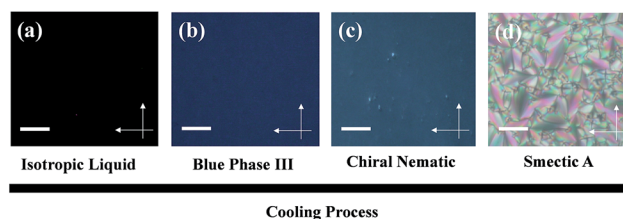


Fig. 2 POM textures of **II-B** upon cooling (0.5 °C min⁻¹). (a) Isotropic state at 100 °C. (b) Blue phase III at 92.1 °C. (c) Chiral nematic phase at 80.2 °C. (d) Smectic A phase at 60.1 °C. (Scale bar: 40 μm. White arrows are the directions of polarizers and analyzers.)

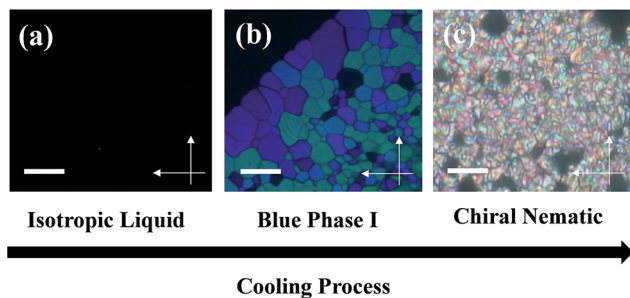


Fig. 3 POM textures of III-D upon cooling (0.5 °C min^{-1}). (a) Isotropic state at 112.3 °C . (b) Blue phase I (platelet textures with different colors and stripes) at 86.2 °C . (c) Chiral nematic phase at 65.1 °C . (Scale bar: $40\text{ }\mu\text{m}$. White arrows are the directions of polarizers and analyzers.)

by a small angle of 10° from the crossed position, the color was changed from blue to light blue (Fig. 4(a)). Upon rotating the polarizer counterclockwise by the same angle (10°) from the crossed position, the color was changed from blue to red (Fig. 4(c)). The POM observations also indicated that the phase of BPIII has selective reflection colors according to their pitch lengths, which were examined by changing the cross angles in the polarizer and analyzer of POM.

Electro-optical studies

In order to investigate the electro-optical switching behavior in the blue phase of diads **II-B** and **III-D**, a rectangular wave function of the AC field at a frequency of 2 kHz was applied to measure the optical transmittance. Fig. 5 shows the voltage-transmittance curve at $T - T_{\text{I-BP}} = -2\text{ °C}$, where the black lines with solid squares and circle squares represent the transmittance of compound **II-B** upon increasing and decreasing voltages, respectively. The red lines with solid dots and circle dots stand for the transmittance of **III-D** upon increasing and decreasing voltages, respectively. Both **II-B** and **III-D** showed enhanced transmittance by increasing the electric field. As transmittance reached 10% and 90% in the V - T curve, we found that **III-D** had higher respective electrical fields (11.5 and $17.2\text{ V }\mu\text{m}^{-1}$) than **II-B** (10.2 and $15.6\text{ V }\mu\text{m}^{-1}$). In addition, in-plane-switching (IPS) cells were utilized to realize the V - T hysteresis by increasing the voltage to saturation. Because hysteresis will influence the grayscale of liquid crystal device, the hysteresis should be minimized for real applications.⁴⁰ The definition of

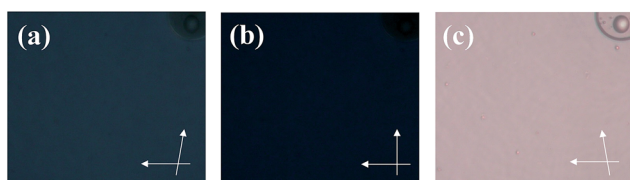


Fig. 4 Optical images of **II-B** observed by POM at 92.7 °C (a) polarizer was rotated clockwise by a small angle of 10° . (b) Polarizer and analyzer were orthogonal. (c) Polarizer was rotated counterclockwise by a small angle of 10° . (White arrows are the directions of polarizers and analyzers.)

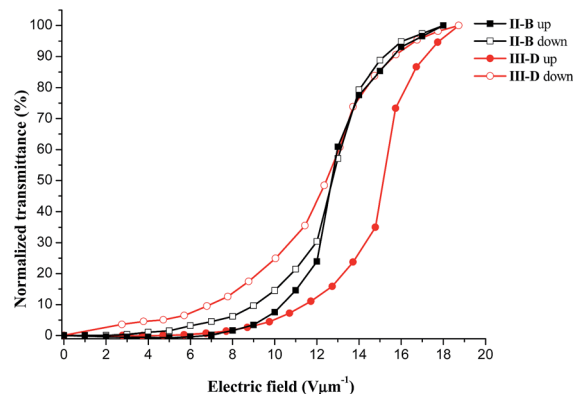


Fig. 5 Optical transmittance of diads **II-B** and **III-D** in BPs (at $T - T_{\text{I-BP}} = -2\text{ °C}$).

hysteresis is $\Delta V/V_{\text{on}}$ (ΔV is the voltage difference between the forward and backward directions at half of the peak transmittance and V_{on} is the driving voltage).⁴¹ The electro-optical switching exhibited that **II-B** did not have any hysteresis ($\sim 0\%$), but **III-D** was observed to have a large hysteresis ($\sim 27\%$). Compared with **II-B**, the higher applied voltages (10% and 90% transmittance in the V - T curve) and hysteresis of **III-D** were due to a larger number of aromatic rings in **III-D** with stronger π - π interactions.

The values of response time for diads **II-B** and **III-D** were obtained from the electro-optical response curves of Fig. S3(a) and (b),[†] respectively (see the ESI). As summarized in Fig. 6, their values of response time were measured with a rectangular wave function of the AC field (at a frequency of 2 kHz) for the rise and decay processes at $T - T_{\text{I-BP}} = -2\text{ °C}$. The definitions of the rise time (τ_{on}) and decay time (τ_{off}) are the response time values for 90% transmittance change by increasing and

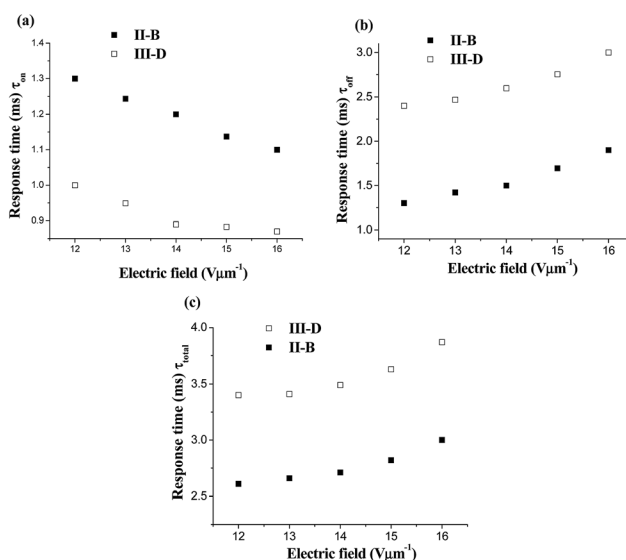


Fig. 6 Diads **II-B** and **III-D** in the BP at $T - T_{\text{I-BP}} = -2\text{ °C}$. (a) Electric-field dependence of the response times for the rise processes. (b) Electric-field dependence of the response times for the decay processes. (c) Electric-field dependence of the total response times.

decreasing voltage, respectively.^{42,43} Both τ_{on} values of **II-B** and **III-D** in Fig. 6(a) were found to be reduced concomitantly by increasing voltage, but their τ_{off} values in Fig. 6(b) are enhanced by increasing voltage. The behaviour of increasing τ_{off} values with higher voltages can be explained by the unwinding helix mode of BPLCs stabilized by a higher voltage which is more difficult to relax back easily *via* the removal of electric fields.⁴⁴ In the meanwhile, we found that the rise time τ_{on} of **III-D** is smaller than **II-B**, but the decay time τ_{off} of **III-D** is larger than **II-B**. Thus, the values of rise time (τ_{on}) and decay time (τ_{off}) have opposite trends for diads **II-B** and **III-D**. As a result, the values of total response time ($\tau_{\text{total}} = \tau_{\text{on}} + \tau_{\text{off}}$) in Fig. 6(c) are enhanced by increasing voltage, which has the same trend as the decay time (τ_{off}) due to the larger values of τ_{off} with more contributions to τ_{total} compared with those of τ_{on} . According to Table S3,[†] the average values of total response time ($\tau_{\text{total}} = \tau_{\text{on}} + \tau_{\text{off}}$) for **II-B** and **III-D** are 2.74 and 3.56 ms, respectively, where **II-B** has the fastest total response time.

According to the definition of the Kerr effect,^{45,46} the formula: $\Delta n_{\text{induced}} = \lambda KE^2$, where Δn is the electric field-induced birefringence, λ is the wavelength of light, K is the Kerr constant and E is the electric-field. The Kerr constants of **II-B** and **III-D** in their corresponding BPs were 2.2×10^{-11} and $2.7 \times 10^{-11} \text{ mV}^{-2}$, respectively, where BPI of **III-D** demonstrated the largest Kerr constant. The BPs with large field-induced birefringences would cause the orientation changes of the ordered molecules easily. In contrast to nitrobenzene with a well-known and large Kerr constant $2.2 \times 10^{-12} \text{ mV}^{-2}$,⁴⁷ **II-B** and **III-D** possessed Kerr constants 10 times larger than nitrobenzene might have useful applications in the future.

Theoretical simulation

As alluded to above, we carried out geometry optimization at the B97D/6-31G(d,p) level for all asymmetrical liquid crystal diads **II-N** ($N = \text{A, B, C}$ and **D**) and **III-N** (where $N = \text{A, B, C}$ and **D**) to analyze the structural variations. The main geometric parameters for the ground states of lowest energy conformations of **II-B**, **III-B** and **III-D** bearing chiral centers at the central linker and/or terminal alkoxy chain are summarized in Table 2 with molecule length, breadth, bent angle and dipole moment, which can influence the temperature range and stabilization of blue phases (BPs). In addition, the related data of the other compounds without BPs are shown in Tables S3–S5 (see ESI[†]).

The front and side views of efficient molecular structures, **III-D**, **III-B** and **II-B** are shown in Fig. 7 and remaining other geometries are shown in the ESI Fig. S4.[†] The biaxiality, bent angle and dipole moment of molecular geometry play a very important role in widening and stabilizing the BP temperature range.⁴⁸ The biaxiality is defined as the ratio of two distinguishable short axes (W_1 , W_2) of the molecule with a flat shape (*i.e.*, possessing a more non-circular cross section), which is different from the uniaxiality with two identical short axes (W). Hence, a similar molecular structure with a more bent shape (*i.e.*, a smaller bent angle in Fig. 7) should have a larger biaxiality (*i.e.*, a larger difference between W_1 and W_2). These parameters are defined as following: L (length along the long axis), biaxiality equals W_1/W_2 (W_1 : width along the short axis normal to the benzene plane and W_2 : width along the short axis parallel to the benzene plane) and bent angles are measured as the angles between the centers of the first, central and final benzene rings of the bent-core structures (see Fig. 7 and Table 2).

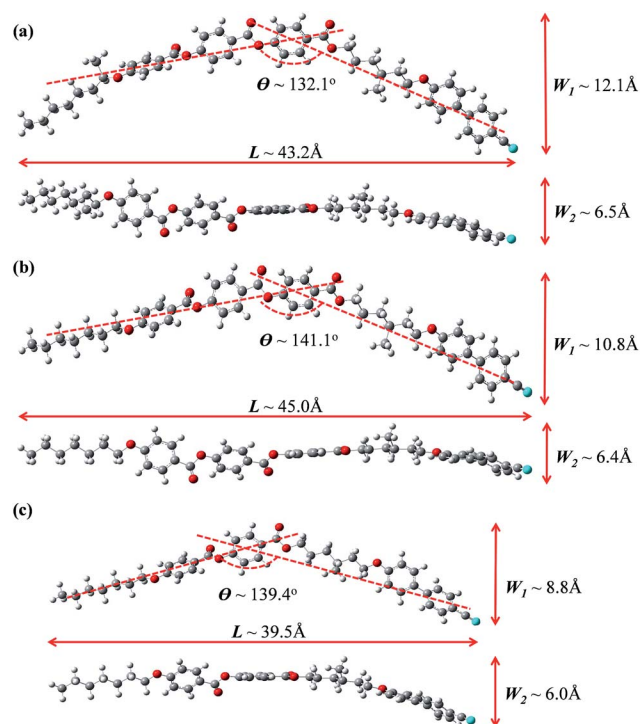


Fig. 7 Molecular models of the lowest energy conformations for single molecules of diads (a) **III-D** (b) **III-B** and (c) **II-B**.

Table 2 Calculated lengths, breadths, bent angles and dipole moments of molecular structures in optimized asymmetrical liquid crystal diads at the B97D level with the 6-31G(d,p) basis set

Compounds	Length L (Å)	Breadth W_1 (Å)	Breadth W_2 (Å)	Biaxial parameter (W_1/W_2)	Bent angle ^a (deg)	Dipole moment (Debye, D)
II-B	39.5	8.8	6.0	1.47	139.4	10.9
III-B	45.0	10.8	6.4	1.69	141.1	13.1
III-D	43.2	12.1	6.5	1.86	132.1	13.2

^a Bent angle (°) measured as the angle between the first, central and final benzene rings' centers of the bent-core structures. The dipole moments of the lowest energy structures are given (see ESI Tables S4–S6).

Comparing the BP temperature range of compound **II-B** and **III-B**, diad **II-B** (~ 3.4 °C) has a little wider BP range than **III-B** (~ 1.5 °C), but diad **III-B** has one more aromatic ring than **II-B**. To explain this result, the difference of biaxiality, dipole moment and bent angle are further investigated between **II-B** and **III-B**. Although the values of biaxiality and dipole moment for diad **III-B** (biaxiality parameter ~ 1.69 and dipole moment ~ 13.1 D) are larger than those of **II-B** (biaxiality parameter ~ 1.47 and dipole moment ~ 10.9 D), diad **II-B** (139.4°) has a more bent shape than **III-B** (141.1°). In this study, we found that the bent shape of molecular geometry is useful to stabilize the BPs so that the BP temperature range of diad **II-B** (~ 3.4 °C) is wider than **III-B** (~ 1.5 °C). On the other hand, diad **III-D** has one more chiral center at the terminal alkoxy chain than **III-B** but the BP temperature range of **III-D** (~ 31.4 °C) is much wider than that of **III-B** (~ 1.5 °C). In order to explain this phenomenon, the differences of biaxiality, dipole moment and bent angle were studied between **III-D** and **III-B**. As shown in Table 2, diad **III-D** (biaxiality parameter ~ 1.86 and dipole moment ~ 13.2 D) has larger values of biaxiality and dipole moment than **III-B** (biaxiality parameter ~ 1.69 and dipole moment ~ 13.1 D). Besides, the molecular geometry of **III-D** (132.1°) is more bent than that of **III-B** (141.1°) so that diad **III-D** (~ 31.4 °C) with a more bent shape (*i.e.*, a larger biaxiality) is observed to have a wide temperature range of BP. In the investigation of biaxiality, bent angle and dipole moment effects on widening and stabilizing the BP temperature range, the large values of biaxiality and dipole moment, along with the bent shape of molecular geometry are found to be useful to extend and stabilize the temperature range of BP.

The electrostatic potential maps of all diads **III-D**, **III-B** and **II-B** calculated at the B97D/6-31G(d,p) level are shown in Fig. 8. The results reveal that the red color refers to the electron-rich

and the blue color refers to more positive charge and thus the green color signifies the zero electrostatic potential. The highest negative potential (red) is always located at the C(O)=O and C=N functionalities. In addition, the remaining electrostatic potential maps of the other diads are also shown in the ESI Fig. S5.†

Conclusions

Two series of novel asymmetrical chiral liquid crystal diads **II-N** (where N = A, B, C, D and E) and **III-N** (where N = A, B, C and D) were synthesized to possess two different mesogenic units which were linked together by an odd-number spacer. The effects of the position of chiral centers and the number of aromatic rings on the mesophasic properties (especially for BPs) were investigated. Among these diads, **II-B** exhibited blue phase III (BPIII) and diads **III-B** and **III-D** revealed blue phase I (BPI), where **III-D** showed the widest temperature of BPI (~ 31 °C). The effects of the number of aromatic rings and the position of chiral centers on the behavior of mesophases, electric-optical properties and Kerr constants were systemically investigated. Based on the molecular modeling, we found that the large values of biaxiality and dipole moment, along with the bent shape of molecular geometry are useful to extend and stabilize the temperature range of BPs. Consequently, the first report of asymmetrical single- and double-chiral liquid crystal diads containing a chiral center at the central linker is illustrated to exhibit BPs, including the mesophases of BPI and BPIII. The single-component discoveries of novel liquid crystal diads with wide BP ranges will pave a new way to optimize BP ranges in the eutectic mixtures for future applications.

Acknowledgements

This project was financially supported by the National Science Council of Taiwan (ROC) through funding (no. NSC 101-2113-M-009-013-MY2 and NSC 102-2221-E-009-174). We are grateful to the National Center for High-performance Computing for computer time and facilities. The powder XRD measurements were supplied by beam-line BL17A (charged by Dr Jey-Jau Lee) of the National Synchrotron Radiation Research Center (NSRRC) in Taiwan.

Notes and references

- 1 N. Podoliak, O. Buchnev, M. Herrington, E. Mavrana, M. Kaczmarek, A. G. Kanaras, E. Stratakis, J. F. Blach, J. F. Henninot and M. Warenghem, *RSC Adv.*, 2014, **4**, 46068–46074.
- 2 W. H. Chen, W. T. Chuang, U. S. Jeng, H. S. Sheu and H. C. Lin, *J. Am. Chem. Soc.*, 2011, **133**, 15674–15685.
- 3 L. J. Chen, C. R. Lee and C. L. Chu, *RSC Adv.*, 2014, **4**, 52804–52807.
- 4 J. M. Wong, J. Y. Hwang and L. C. Chien, *Soft Matter*, 2011, **7**, 7956–7959.
- 5 A. Yoshizawa, *RSC Adv.*, 2013, **3**, 25475–25497.

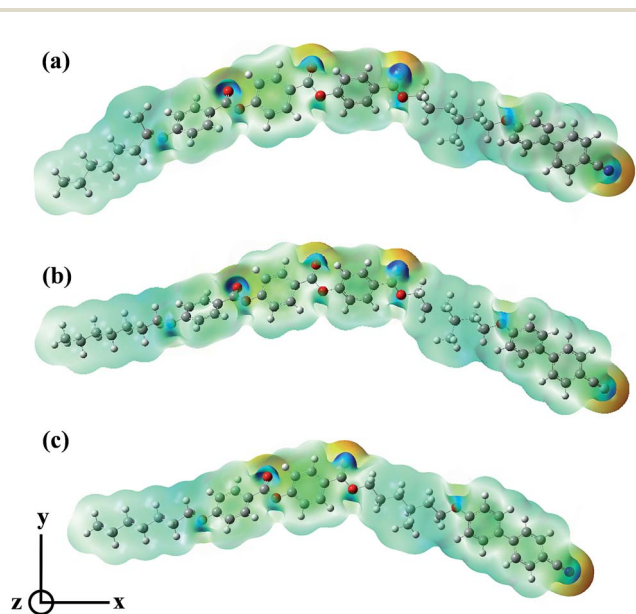


Fig. 8 Molecular electrostatic potentials mapped on the electron densities of the lowest energy structures for the three asymmetrical liquid crystal diads: (a) **III-D**, (b) **III-B** and (c) **II-B**.

- 6 O. Jin, D. Fu, J. Wei, H. Yang and J. Guo, *RSC Adv.*, 2014, **4**, 28597–28600.
- 7 H. Stegemeyer, Th. Blumel, K. Hiltrop, H. Onusseit and F. Porsch, *Liq. Cryst.*, 1986, **1**, 3–28.
- 8 E. Dubois-Violette and B. Pansu, *Mol. Cryst. Liq. Cryst.*, 1988, **165**, 151–182.
- 9 J. A. N. Zasadzinski, S. Meiboom, M. J. Sammon and D. W. Berreman, *Phys. Rev. Lett.*, 1986, **57**, 364–367.
- 10 O. Henrich, K. Stratford, M. E. Cates and D. Marenduzzo, *Phys. Rev. Lett.*, 2011, **106**, 107801-1–107801-4.
- 11 A. J. Yoshizawa, *Soc. Inf. Disp.*, 2008, **16**, 1189–1194.
- 12 K. M. Chen, S. Gauza, H. Xianyu and S. T. Wu, *J. Disp. Technol.*, 2010, **6**, 318–322.
- 13 H. Kikuchi, M. Yokota, Y. Hisakado, H. Yang and T. Kajiyama, *Nat. Mater.*, 2002, **1**, 64–68.
- 14 Y. H. Lin, H. S. Chen, H. C. Lin, Y. S. Tsou, H. K. Hsu and W. Y. Li, *Appl. Phys. Lett.*, 2010, **96**, 113505-1–113505-3.
- 15 Y. H. Lin, H. S. Chen, T. H. Chiang, C. H. Wu and H. K. Hsu, *Opt. Express*, 2011, **19**, 2556–2561.
- 16 L. Rao, Z. Ge, S. Gauza, K. M. Chen and S. T. Wu, *Mol. Cryst. Liq. Cryst.*, 2010, **527**, 186–197.
- 17 Z. Ge, S. Gauza, M. Jiao, H. Xianyu and S. T. Wu, *Appl. Phys. Lett.*, 2009, **94**, 101104-1–101104-3.
- 18 W. He, G. Pan, Z. Yang, D. Zhao, G. Niu, W. Huang, X. Yuan, J. Guo, H. Cao and H. Yang, *Adv. Mater.*, 2009, **21**, 2050–2053.
- 19 Y. Shi, X. Wang, J. Wei, H. Yang and J. Guo, *Soft Matter*, 2013, **9**, 10186–10195.
- 20 H. J. Coles and M. N. Pivnenko, *Nature*, 2005, **436**, 997–1000.
- 21 M. Tanaka and A. Yoshizawa, *J. Mater. Chem. C.*, 2013, **1**, 315–320.
- 22 S. Taushanoff, K. Van Le, J. Williams, R. J. Twieg, B. K. Sadashiva, H. Takezoe and A. Jákli, *J. Mater. Chem.*, 2010, **20**, 5893–5898.
- 23 M. Lee, S. T. Hur, H. Higuchi, K. Song, S. W. Choi and H. Kikuchi, *J. Mater. Chem.*, 2010, **20**, 5813–5816.
- 24 I. Dierking, W. Blenkhorn, E. Credland, W. Drake, R. Kociuruba, B. Kayser and T. Michael, *Soft Matter*, 2012, **8**, 4355–4362.
- 25 B. Li, W. He, L. Wang, X. Xiao and H. Yang, *Soft Matter*, 2013, **9**, 1172–1177.
- 26 H. Ocak, B. Bilgin-Eran, M. Prehm, S. Schymura, J. P. F. Lagerwall and C. Tschierske, *Soft Matter*, 2011, **7**, 8266–8280.
- 27 M. Sato, A. Yoshizawa and F. Ogasawara, *Mol. Cryst. Liq. Cryst.*, 2007, **475**, 99–112.
- 28 J. Ban, S. Chen and H. Zhang, *RSC Adv.*, 2014, **4**, 54158–54167.
- 29 C. V. Yelamaggad, N. L. Bonde, A. S. Achalkumar, D. S. S. Rao, S. K. Prasad and A. K. Prajapati, *Chem. Mater.*, 2007, **19**, 2463–2472.
- 30 A. Yoshizawa, Y. Kogawa, K. Kobayashi, Y. Takanishi and J. Yamamoto, *J. Mater. Chem.*, 2009, **19**, 5759–5764.
- 31 C. V. Yelamaggad, V. P. Tamilenthir, D. S. S. Rao, G. G. Nair and S. K. Prasad, *J. Mater. Chem.*, 2009, **19**, 2906–2908.
- 32 C. V. Yelamaggad, G. Shanker, U. S. Hiremath and S. K. Prasad, *J. Mater. Chem.*, 2008, **18**, 2927–2949.
- 33 A. T. M. Marcelis, A. Koudijs, Z. Karczmarzyk and E. J. R. Sudhölter, *Liq. Cryst.*, 2003, **30**, 1357–1364.
- 34 T. Donaldson, H. Staesche, Z. B. Lu, P. A. Henderson, M. F. Achard and C. T. Imrie, *Liq. Cryst.*, 2010, **37**, 1097–1110.
- 35 S. Aya, A. Zep, K. Aihara, K. Ema, D. Pocięcha, E. Gorecka, F. Araoka, K. Ishikawa and H. Takezoe, *Opt. Mater. Express*, 2014, **4**, 662–671.
- 36 I. H. Chiang, C. J. Long, H. C. Lin, W. T. Chuang, J. J. Lee and H. C. Lin, *ACS Appl. Mater. Interfaces*, 2014, **6**, 228–235.
- 37 S. J. Grimme, *J. Comput. Chem.*, 2006, **27**, 1787–1799.
- 38 B. H. Besler, K. M. Merz Jr and P. A. Kollman, *J. Comput. Chem.*, 1990, **11**, 431–439.
- 39 M. J. Frisch, G. W. Trucks and H. B. Schlegel, *et al.*, *Gaussian 09, Revision A.1*, Gaussian, Inc., Wallingford CT, 2009.
- 40 K. M. Chen, S. Gauza, H. Xianyu and S. T. Wu, *J. Disp. Technol.*, 2010, **6**, 318–322.
- 41 H. Y. Chen, J. L. Lai, C. C. Chan and C. H. Tseng, *J. Appl. Phys.*, 2013, **113**, 123103-1–123103-4.
- 42 L. Rao, J. Yan, S. T. Wu, Y. C. Lai, Y. H. Chiu, H. Y. Chen, C. C. Liang, C. M. Wu, P. J. Hsieh, S. H. Liu and K. L. Cheng, *J. Disp. Technol.*, 2011, **7**, 627–629.
- 43 J. Yan and S. T. Wu, *J. Disp. Technol.*, 2011, **7**, 490–493.
- 44 H. Y. Chen, J. L. Lai, C. C. Chan and C. H. Tseng, *J. Appl. Phys.*, 2013, **113**, 123103-1–123103-4.
- 45 L. Rao, J. Yan, S. T. Wu, S. Yamamoto and Y. Haseba, *Appl. Phys. Lett.*, 2011, **98**, 081109-1–081109-3.
- 46 Y. Hisakado, H. Kikuchi, T. Nagamura and T. Kajiyama, *Adv. Mater.*, 2005, **17**, 96–98.
- 47 S. W. Choi, S. I. Yamamoto, Y. Haseba, H. Higuchi and H. Kikuchi, *Appl. Phys. Lett.*, 2008, **92**, 043119-1–043119-3.
- 48 L. Wang, W. He, M. Wang, M. Wei, J. Sun, X. Chen and H. Yang, *Liq. Cryst.*, 2013, **40**, 354–367.